Mathematical Modelling and Analysis
Volume 29, Issue 4, 600–620, 2024
https://doi.org/10.3846/mma.2024.18963

Modelling for a New Mechanical Passive Damper and its Mathematical Analysis

Dai Watanabe[a] **and Shuji Yoshikawa**[b]

[a] *College of Systems Engineering and Science, Shibaura Institute of Technology*
307 Fukasaku, Minuma-ku, Saitama City, 337-8570 Saitama, Japan
[b] *Division of Mathematical Sciences, Faculty of Science and Technology, Oita University*
700 Dannoharu, Oita-shi, 870-1192 Oita, Japan
E-mail(*corresp.*): yoshikawa@oita-u.ac.jp
E-mail: dai-wata@shibaura-it.ac.jp

Received April 13, 2023; accepted February 22, 2024

Abstract. To improve ride comfort, an oil damper should restrain its damping force in a high-velocity range. A lot of dampers with such properties were developed. For example, the one controlling the flux of oil by a leaf valve is widely adapted and reasonable. However, it is difficult to represent its dynamics with a simple mathematical model, and the cost of a computational fluid dynamics is too expensive. To overcome the disadvantages, the first author in [15] developed the other mechanical oil damper with sub-pistons instead of the leaf valve, which enabled us to propose a simple mathematical model with linear ordinary differential equations, thanks to the simple mechanism to control the oil flow. In this article, we give a more detailed mathematical model for the damper taking the dynamic pressure resistance into account, which is represented by nonlinear ordinary differential equations. In addition, a numerical scheme for the model is also proposed and its mathematical analysis such as the validity of the numerical solutions is shown.

Keywords: oil damper, mathematical modelling, nonlinear differential equations, structure-preserving numerical methods.

AMS Subject Classification: 65L70; 74D99.

1 Introduction

Oil dampers used in automobile suspensions generate damping force by utilizing the resistance passing oil in a cylinder through a narrow channel in the

piston. Hence, the damping force generated by the damper depends on the speed of the piston. It is known experimentally that the damping force of a simple normal damper is proportional to the speed of the piston. Thus, it will act stiffly especially against unsteady fast inputs if we make the damping force strong relative to the speed, whereas the convergence of vibration phenomena will deteriorate if we simply weaken the damping force. In order to satisfy these conflicting demands, various mechanisms have been developed to adjust the damping force generated by dampers. An reasonable and widely adopted mechanism is that has a leaf valve installed at the outlet of the flow path ([4]). This is based on the fact that the stroke is relatively fast in situations where people feel uncomfortable, such as when riding on uneven ground or when going over steps, and the stroke is slow when the vehicle is moving, such as pitching or rolling. When the operating speed is high, the fluid displaces the leaf valve and flows while opening the flow path, making the damping force characteristics nonlinear. There are also dampers that can exert a damping force suitable for the driving mode by electrically controlling the flow path of the damper, and dampers that use MR fluid to control the damping force by applying a magnetic field to the oil ([3, 11]), those using a complex mechanism in the piston structure to exert damping force according to the input frequency ([8]), and even electromagnetic dampers that do not use oil have been developed ([10]). Dampers in automobiles, like suspension springs, are important elements that characterize the vehicle's ride comfort and dynamic characteristics. Therefore, in vehicle development, it is necessary to fully consider what kind of damping characteristics should be given to the damper in order to satisfy the performance of the vehicle. It is also important to be able to reproduce it. Thus, research has been conducted on methods for analytically determining the damping coefficient of oil dampers (e.g., [5, 12, 14]). However, when modeling a damper with a general piston equipped with a leaf valve type damping force adjustment mechanism, it is difficult to accurately identify the damping parameters that represent the characteristics of the damper. This is due to the difficulty of predicting the behavior of the leaf valve during its stroke and the constantly changing flow path. Herr et al. [9] and Shams et al. [13] attempted to identify the damping parameters of a damper using computational fluid dynamics (CFD). However, because these CFD methods require expensive calculation costs, it is not realistic to use them for designing the damping characteristics of dampers. Therefore, one of the authors proposed a novel damper with a ring flow path piston mechanism that has a large damping force adjustment function, and at the same time, proposed a damper that is as simple as possible so that the damping force of the damper can be calculated sequentially in real time when applying damper characteristics to a vehicle model. We have been modeling a damper expressed by an equation([15]). It was also confirmed that the proposed damper model was in good agreement with experimental data. The mechanism of the proposed model is simple, only adding movable subpistons P_u and P_l attached to the main piston P_m with rods through springs with spring constants K_u and K_l, as shown in Figure 1 below. These subpistons play roles in adjusting the flow paths of the main damper in response to its expansion and contraction. Namely, the tapered parts attached to the

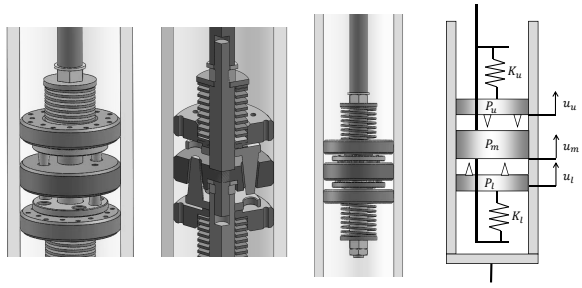

Figure 1. CAD models of the damper and its simplified image.

sub-pistons adjust the flow paths of the main piston. During compression, the upper piston enlarges the flow paths to reduce resistance. On the other hand, during extension, the lower piston enlarges the flow paths to reduce resistance. The design is such that the resistance force decreases by the opening of the flow channel by the upper piston during compression and by the opening of the flow channel by the lower piston during extension.

Since this damper has a simple structure and its variable resistance function is passive, it does not require electric power or other power and is expected to improve durability. Furthermore, the damping characteristics can be easily modeled since it is designed with mathematical modeling in mind.

In this paper, we first construct the mathematical model in Section 2. In the previous work of the first author [15], a mathematical model for this damper has already been proposed, but it is a linearized approximate model that does not take into account the effect of dynamic pressure resistance (also called hydrodynamic resistance). The dynamic pressure resistance is a natural resistance force arising from the hydrodynamic properties of the oil, and should be determined by the oil flow inside the damper. However, it is theoretically difficult to obtain the resistance force by the precise analysis for the flow of viscous fluid against a complex shape of a domain, including the flow path on the piston inside the damper, and it is also inefficient to consider a numerical simulation following the fluid dynamics. Therefore, damper models usually adopt many approximations, and under the assumptions of these approximations, several constants are derived empirically or experimentally. The flow paths of the sub-pistons are tube-shaped, and the resistance force to the tube-shaped channel is well known. On the other hand, the flow paths of the main piston have tapered-shaped that is adjusted by a tapered (or conical) controller, so it is necessary to propose some new model appropriate for these tapered-shaped flow paths. More precisely, we need to determine how the pressure difference in each channel contributes to the dynamic pressure resistance on the main piston. As we mention in Section 2, we propose the new model under the hypothesis that "the proportion of the cross-sectional area contributed by the pressure difference is equal to the proportion of each flow rate." The validity of our model proposed here is guaranteed with high accuracy by comparison with the experimental data obtained by CFD methods.

Section 3 is devoted to a mathematical analysis of the numerical solution of the mathematical model obtained here. The obtained mathematical model is an ordinary differential equation but nonlinear, by taking the dynamic pressure resistance into account. Since the nonlinear term belongs to $C^{1,1}$, the existence and uniqueness of the solution are assured by the classical Cauchy's existence theorem (e.g., [1, 2], etc.). Here we investigate the behavior of the solution through numerical simulations. Although highly accurate numerical methods for ordinary differential equations, such as the Runge-Kutta method, are well known [7], their accuracy is not assured for nonlinear terms that are not sufficiently regular such as our model introduced here. Therefore, in this article, we apply the structure-preserving numerical method. The numerical methods that inherit a structure for the original differential equation in some sense are called the structure-preserving numerical methods. The inherited structures are e.g., symplectic structures (see e.g., [7]), energy structures, the positivity of solutions, and so on. We here focus on the energy structure as introduced in [6]. The energy structure, such as the energy conservation law, is often utilized to show the stability of the numerical solution, and the property can also be applied for the error estimate (e.g., [16, 17]). We will derive a structure-preserving numerical method for this mathematical model, introduce the algorithm to calculate the numerical solution, and show the error estimate between the numerical solution and the exact solution.

In Section 4, we demonstrate several numerical simulations using this algorithm and explain that the mathematical model satisfies the expected properties of the damper. In the last section, the results obtained in this paper are summarized as a conclusion.

2 Mathematical model for the proposed damper

As introduced in the previous section, the damper proposed in this article is a system in which the flow path of the central piston (main piston) is adjusted by a sub-piston called a variable flow valve (VFV) controller, as shown in the figure in the previous section (Figure 1). The main-piston is placed between two sub-pistons, and is fixed to the rod from the top. The sub-pistons are not directly fixed to the rod but are connected to it through springs to allow variable distance from the main-piston. Let us explain each piston in more detail. As shown in Figure 2, the main piston P_m has tapered flow channels, and the sub-pistons P_u and P_l have tube-shaped flow channels. The tapered flow channels in the main piston are adjusted in its flow rate by conical components fixed to the sub-piston.

When compressing the damper, the flow paths of the main piston, which are adjusted by the sub-piston on the upper side in relation to the main piston, are enlarged. On the other hand, when extending the damper, the flow paths of the main piston, which are adjusted by the sub-piston on the lower side, are enlarged. Next, we consider a model for the resistance force on each of the sub-pistons and the main piston.

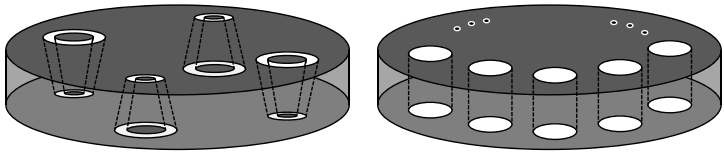

(a) main-piston (b) sub-piston

Figure 2. Shape of flow channel.

2.1 Resistance force for sub-piston

In this subsection, we first focus on one sub-piston (VFV controller) and derive an expression for the resistance force on it. Let V_s be the velocity of the target sub-piston and A_s be its cross-sectional area.

It is known that the resistance force of the damper arises from the pressure difference at the exit and entrance of the piston. The flow path of the sub-piston has a simple tubular shape as shown on the right in Figure 2, and the viscous and dynamic pressure resistances in this case are well known, namely, from the Hagen-Poiseuille equation, the pressure difference δp_{sv} at both ends resulting from the viscous resistance of a single tubular channel of radius r_s and length L_s with viscosity μ and flow rate q_s is given by $\delta p_{sv} = \frac{8\mu L_s}{\pi r_s^4} q_s$, and the pressure difference δp_{sk} at both ends resulting from the dynamic pressure resistance of a single tube-type channel is known to be given by $\delta p_{sk} = \frac{\rho}{2C_d^2} v_s^2$, where ρ is the density of oil and v_s is the average velocity at the channel exit. Note that C_d is a constant called the orifice flow coefficient, which is often taken values between 0.7 and 1. The formula corresponds to the Bernoulli law $\delta p = \frac{\rho}{2} v_s^2$ adjusted empirically by the flow coefficient C_d to account for the flow reduction and friction loss. Although C_d is originally determined from various conditions such as fluid equations, domain and channel geometry, it is theoretically and numerically unrealistic to analyze fluid equations on a complicated geometry and a moving domain, and the above empirical law has been used for a long time.

Since the sub-piston consists of more than one of these tube-shaped channels, the resistance force in that case is obtained as follows. Let n_s be the number of channels in the sub-piston, Q_s the flow rate of the entire sub-piston, and F_{sv} the force due to a viscous resistance on the sub-piston. Then the relation $Q = nq$, $F_{sk} = A_s \delta p_{sv}$, $Q_s = A_s V_s$ holds. Therefore, we obtain

$$F_{sv} = -\frac{8\mu L_s A_s^2}{n_s \pi r_s^4} V_s.$$

Similarly, since the cross-sectional area of one channel is πr_s^2 and the flow rate of n_s channels is $n_s \pi r_s^2 v_s$, we see that $A_s V_s = n_s \pi r_s^2 v_s$. Let us denote the force consisting of a dynamic pressure resistance by F_{sk}. Since the relation $F_{sk} = A_s \delta p_{sk}$ holds, we have

$$F_{sk} = -\frac{\rho A_s^3}{2C_d^2 n_s^2 \pi^2 r_s^4} |V_s| V_s,$$

where we take the direction of force into account. Therefore, the total force F_s on the sub-piston is derived as

$$F_s = F_{sv} + F_{sk} = -\frac{8\mu L_s A_s^2}{n_s \pi r_s^4} V_s - \frac{\rho A_s^3}{2C_d^2 n_s^2 \pi^2 r_s^4} |V_s| V_s. \tag{2.1}$$

2.2 Resistance force on the main-piston

Next, we shall derive the resistance force on the main-piston. The main-piston is sandwiched from both sides by the sub-pistons, and its flow rate is adjusted by the sub-pistons. The conical-shaped components are attached to the sub-pistons and adjust the sizes of the flow paths of the main-piston. To derive the force on the main-piston is somewhat complicated due to the tapered shape of the flow channel. Let V_m, A_m, and L_m denote the speed, cross-sectional area, and thickness of the main piston, respectively.

Note that the contracting (or extensional, resp.) side flow path is not completely closed during the extensional (or contracting, resp.) stroke. The flow paths of the main-piston are variable, and when the main-piston extends ($V_m \geq 0$), oil flows in a negative direction (Figure 3), and when the main-piston contracts ($V_m \leq 0$), oil flows in a positive direction (Figure 4). Thus, the direction of oil flow in the main-piston depends on the sign of V_m.

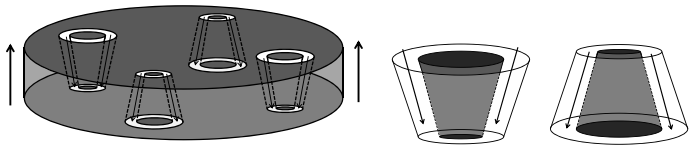

Figure 3. The direction of oil flow when the main-piston extends.

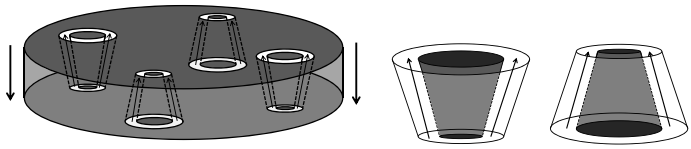

Figure 4. The direction of oil flow when the main-piston contracts.

First, we focus on the equations for the viscous and dynamic pressure resistances on a single tapered flow channel. Suppose that the sub-piston moves from its initial position and the channel width is t as shown in Figure 5. Let $\tilde{x}$ be a new coordinate system parallel to x with the bottom of the piston at 0 and $\tilde{y}$ be parallel to y with the center of the channel at 0. Let $R(\tilde{x})$ denote the distance from the center of the tapered channel at $\tilde{x}$, $R(0) = R_0$ and $R(L) = R_1$. Note that for given R_0 and R_1, $R(\tilde{x}) = \frac{R_1 - R_0}{L}\tilde{x} + R_0$.

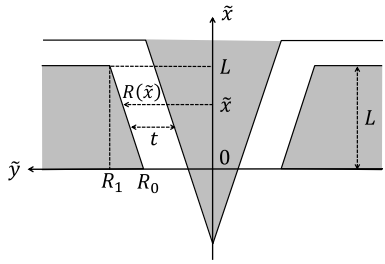

Figure 5. A taper-shaped fluid path.

It is known that the dynamic pressure resistance is given by the following formula as well as that of a tubular fluid path, namely, the pressure loss by the dynamic pressure δp_k is given by

$$\delta p_k = \frac{\rho}{2C_d^2} v_m^2. \tag{2.2}$$

On the other hand, viscous resistance is different from the one for the tubular shaped channel, because it depends on the shape of the channel. The dynamics for the incompressive fluid is represented by the Navier-Stokes equation:

$$\frac{\partial \boldsymbol{v}}{\partial t} + \boldsymbol{v} \cdot \nabla \boldsymbol{v} = -\frac{1}{\rho}\nabla p + \frac{\mu}{\rho}\Delta \boldsymbol{v}.$$

Here, the damper is symmetric with respect to the rod of piston, then we assume that the flow is regarded as two-dimenional one. In the two-dimensional flow $\boldsymbol{v} = (v_{\tilde{x}}, v_{\tilde{y}})$, the equation for $\tilde{x}$-direction is denoted by

$$\frac{\partial v_{\tilde{x}}}{\partial t} + \left(v_{\tilde{x}} \frac{\partial v_{\tilde{x}}}{\partial \tilde{x}} + v_{\tilde{y}} \frac{\partial v_{\tilde{y}}}{\partial \tilde{y}} \right) = -\frac{1}{\rho}\frac{\partial p}{\partial \tilde{x}} + \frac{\mu}{\rho}\Delta v_{\tilde{x}}.$$

Here, we assume the flow is layered and steady flow. Even under the steady flow assumption, the left hand side is not negligible, in general. However, in our model, we assume the left hand side is neglected, because the difference between the cross-sectional areas of entry and exit is not so large in addition to the fact that the viscous force is dominant compared to the inertial force. We may thus consider the steady state $\frac{\partial p}{\partial \tilde{x}} = \mu \Delta v_{\tilde{x}}$. Moreover, since the layer flow assumption implies $p(\tilde{x}, \tilde{y}) = p(\tilde{x})$ and $v_{\tilde{x}}(\tilde{x}, \tilde{y}) = v_{\tilde{x}}(\tilde{y})$, we can rewrite the equation to $\frac{dp}{d\tilde{x}} = \mu \frac{d^2 v_{\tilde{x}}}{d\tilde{y}^2}$. Under the boundary conditions $v_{\tilde{x}}(R) = 0$ and $v_{\tilde{x}}(R - t) = 0$, the above equation is solved explicitly as

$$v_{\tilde{x}}(\tilde{y}) = \frac{1}{2\mu} \left\{ \tilde{y}^2 - (2R - t)\tilde{y} + R^2 - tR \right\} \frac{dp}{d\tilde{x}}. \tag{2.3}$$

The flux q for a tapered fluid path can be obtained by integrating (2.3) over the cross section as follows:

$$q = \pi(2R - t) \int_{R-t}^{R} v_{\tilde{x}}(\tilde{y}) d\tilde{y} = \frac{\pi}{12\mu}(2R - t)t^3 \frac{dp}{d\tilde{x}}.$$

Therefore, the pressure difference δp_v between both edges due to the viscous resistance is given by

$$\delta p_v = \int_{p(0)}^{p(L)} dp = \frac{12\mu q}{\pi t^3} \int_0^L \frac{1}{2R - t} d\tilde{x}. \tag{2.4}$$

Substituting $R = R(\tilde{x}) = \frac{R_1 - R_0}{L}\tilde{x} + R_0$ into (2.4) yields

$$\delta p_v = \frac{6\mu L}{\pi t^3 (R_1 - R_0)} \log\left\{ \frac{2(R_1 - R_0)}{2R_0 - t} + 1 \right\} q.$$

Now, from the geometrical structure of the fluid path (Figure 5), we impose the constraints that $\min\{R_0, R_1\} \geq t$ and $\min\{R_0, R_1\} > 0$, and hence $2\min\{R_0, R_1\} > t$. Therefore, the following relation holds

$$\frac{2(R_1 - R_0)}{2R_0 - t} + 1 > 0.$$

In the above argument for the viscous resistance on the taper-shaped path, we have not specifically mentioned the direction of flow. Observe that when $V_m \geq 0$, the oil flows from top to bottom with $q \leq 0$ (i.e., $\delta p_v \leq 0$), and when $V_m \leq 0$, the oil flows from bottom to top with $q \geq 0$ (i.e., $\delta p_v \geq 0$).

Next, let us derive a formula for the resistance force on the main piston consisting of multiple taper-shaped flow paths, from the viscous and dynamic pressure resistances of one taper-shaped flow path given above. We then derive an expression for the resistance force on the main piston consisting of multiple channels. As shown in Figure 7 given below, the main piston P_m is distinguished by a subscript m, the upper sub-piston P_u by u, and the lower sub-piston P_l by l. The effect of gravity is neglected here. From the geometric structure of the flow paths, it is obviously seen that $R_{0u} < R_{1u}$ and $R_{0l} > R_{1l}$. Assume that the main piston has n_u channels whose flows are controlled by P_u and n_l channels whose flows are controlled by P_l. Then the flow Q_m of the main piston is equal to $n_u q_u + n_l q_l$.

Let us first derive the resistance force F_{mv} arising from the viscous resistance to the main piston. From the resistance force for one taper-shaped fluid path, flow rates by the viscous resistance are given as $q_u = \phi_u \delta p_v$, $q_l = \phi_l \delta p_v$, where we set

$$\phi_r := \frac{\pi(R_{1u} - R_{0u})t_u^3}{6\mu L_m \log\left(\frac{2(R_{1u} - R_{0u})}{2R_{0u} - t_u} + 1\right)}, \quad \phi_l := \frac{\pi(R_{1l} - R_{0l})t_l^3}{6\mu L_m \log\left(\frac{2(R_{1l} - R_{0l})}{2R_{0l} - t_l} + 1\right)}. \tag{2.5}$$

We thus obtain the relation between the total flow Q_m and the pressure difference as follows:

$$\begin{aligned} Q_m &= (n_u\phi_u + n_l\phi_l)\delta p_v \\ &= \frac{\pi}{6\mu L}\left\{ \frac{(R_{1u} - R_{0u})t_u^3}{\log\left(\frac{2(R_{1u} - R_{0u})}{2R_{0u} - t_u} + 1\right)} n_u + \frac{(R_{1l} - R_{0l})t_l^3}{\log\left(\frac{2(R_{1l} - R_{0l})}{2R_{0l} - t_l} + 1\right)} n_l \right\} \delta p_v. \end{aligned}$$

Let us denote the force to main piston by viscous resistance by F_{mv}, respectively. Substituting $Q_m = A_m V_m$ and $F_{mv} = A_m \delta p_v$ into the above equation implies

$$\begin{aligned} F_{mv} &= -\frac{A_m^2}{(n_r\phi_r + n_l\phi_l)} V_m \\ &= -\frac{6\mu L_m A_m^2}{\pi \left\{ \frac{(R_{1u}-R_{0u})t_u^3}{\log\left(\frac{2(R_{1u}-R_{0u})}{2R_{0u}-t_u}+1\right)} n_u + \frac{(R_{1l}-R_{0l})t_l^3}{\log\left(\frac{2(R_{1l}-R_{0l})}{2R_{0l}-t_l}+1\right)} n_l \right\}} V_m. \end{aligned}$$

Let us next derive the resistance force F_{mk} on the main-piston by the dynamic pressure resistance. The pressure difference due to dynamic pressure resistance is given by (2.2). However, the pressure difference differs because the flow velocity differs between the flow path controlled by the piston P_u and the one by P_l. Here, we propose the simple model:

Ratio of cross sectional area contributed by pressure difference equals ratio of each flow rate. (2.6)

Namely, the composite resistance force contributed by the pressure difference from one channel is denoted by

$$F_{ku} = -\frac{\rho}{2C_d^2} A \frac{q_u}{Q}, \quad F_{kl} = -\frac{\rho}{2C_d^2} A \frac{q_l}{Q}.$$

Remark that to propose (2.6) is one of our purposes of this article. The validity of this model is ensured in the CFD-tests. In order to confirm the validity of the proposed model equations for damping force due to viscous and dynamic pressure resistance, we compare with the data of a numerical fluid dynamics analysis. The graphs show a comparison of the damping force calculated by the model equation with a steady-state flow analysis performed with a sub-piston lift varying from 2[mm] to 6[mm] and a flow velocity corresponding to the piston speed in increments of 0.02[m/s]. As shown in the graph (Figure 6), the CFD results and the damping force calculated by the model equation are compared with each other. As this graph shows, there is a good correspondence between the CFD results and the results calculated by the proposed model.

The total flow Q_m on the main-piston satisfies $Q_m = n_u q_u + n_l q_l = (n_u\phi_u + n_l\phi_l)\delta p_m$. Then we see that

$$q_u = \frac{\phi_u}{n_u\phi_u + n_l\phi_l} Q_m, \quad q_l = \frac{\phi_l}{n_u\phi_u + n_l\phi_l} Q_m.$$

Denote the area of exit of compression and tension by a_u and a_l, respectively. Then we have $q_u = a_u v_u$ and $q_l = a_l v_l$. It follows from $Q_m = A_m V_m$ that

$$F_{ku} = -\frac{n_u \rho A_m^3}{2C_d^2 a_u^2} \left(\frac{\phi_u}{n_u\phi_u + n_l\phi_l} \right)^3 V_m^2, \quad F_{kl} = -\frac{n_l \rho A_m^3}{2C_d^2 a_l^2} \left(\frac{\phi_l}{n_u\phi_u + n_l\phi_l} \right)^3 V_m^2.$$

Therefore, dynamic pressure is given by

$$\begin{aligned} F_{mk} &= F_{ku} + F_{kl} \\ &= -\frac{\rho A_m^3}{2C_d^2} \left\{ \frac{n_u}{a_u^2} \left(\frac{\phi_u}{n_u\phi_u + n_l\phi_l} \right)^3 + \frac{n_l}{a_l^2} \left(\frac{\phi_l}{n_u\phi_u + n_l\phi_l} \right)^3 \right\} |V_m| V_m. \end{aligned}$$

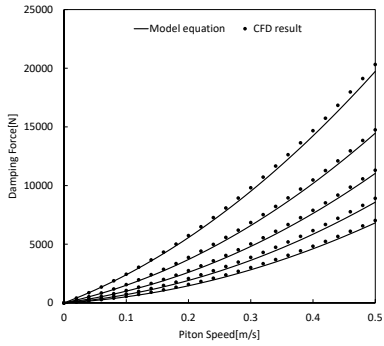

Figure 6. Validity through the comparison between (2.6) and CFD.

Here, we have to pay attention to the exit areas a_u and a_l. Namely, as mentioned above, the oil direction is different by the sign of V_m, which means that a_u and a_l take other values by the sign of V_m.

2.3 Input and output of damper

Let u_m, u_u, and u_l be the displacements of the main piston, the upper sub-piston, and the lower sub-piston, respectively. We want to find the force (output) F_d of the damper for a given input u_m. We can use $\partial_t u_m$ as the velocity V_m of the main piston in the previous section, and $\partial_t u_u$ for the upper sub-piston P_u and $\partial_t u_l$ for the lower sub-piston P_l to the velocity V_s of the sub-piston.

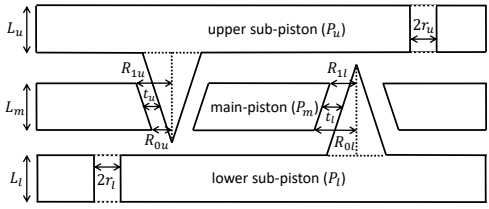

Figure 7. Simplified image of damper.

As shown in Figure 7, let L_m be the thickness of the main-piston and L_u and L_l be the thicknesses of the sub-pistons. The sub-pistons P_u and P_l are spaced a little from the main piston so that t_u and $t_l > 0$, respectively. Fix P_m to the piston rod with a spring of spring constants K_u and K_l so that the natural length of P_m is fixed to the piston rod. Then, the forces on the upper and lower sub-pistons due to the springs are given by $-K_u(u_u - u_m)$ and $-K_l(u_l - u_m)$, respectively. Neglecting the effect of gravity, the forces on the sub-piston are only the resistance force of the damper given by (2.1) and the repulsive force of the spring. Therefore, the equations of motion of the

sub-piston are

$$M_u\partial_t^2 u_u + C_u\partial_t u_u + \tilde{C}_u|\partial_t u_u|\partial_t u_u + K_u\,(u_u - u_m) = 0, \tag{2.7}$$

$$M_l\partial_t^2 u_l + C_l\partial_t u_l + \tilde{C}_l|\partial_t u_l|\partial_t u_l + K_l\,(u_l - u_m) = 0, \tag{2.8}$$

where M_r and M_l are the masses of P_r and P_l, and from (2.1) the damper resistance constants are given by

$$C_u = \frac{8\mu L_u A_u^2}{n_u\pi r_u^4}, \quad C_l = \frac{8\mu L_l A_l^2}{n_l\pi r_l^4}, \quad \tilde{C}_u = \frac{\rho A_u^3}{2C_d^2 n_u^2\pi^2 r_u^4}, \quad \tilde{C}_l = \frac{\rho A_l^3}{2C_d^2 n_l^2\pi^2 r_l^4}.$$

The output force F_d is represented by u_r and u_l, that is,

$$\begin{aligned} F_d = &\left(C_m\partial_t u_m + \tilde{C}_m|\partial_t u_m|\partial_t u_m\right) + \left(C_u\partial_t u_u + \tilde{C}_u|\partial_t u_u|\partial_t u_u\right) \\ &+ \left(C_l\partial_t u_l + \tilde{C}_l|\partial_t u_l|\partial_t u_l\right), \end{aligned} \tag{2.9}$$

where we remark that C_m and $\tilde{C}_m$ are not constants but nonlinear coefficients depending on u_m, u_u, and u_l such as

$$C_m(u_m, u_u, u_l) := \frac{A_m^2}{n_u\phi_u + n_l\phi_l}, \tag{2.10}$$

$$\tilde{C}_m(u_m, u_u, u_l) := \frac{\rho A_m^3}{2C_d^2}\left\{\frac{n_u}{a_u^2}\left(\frac{\phi_u}{n_u\phi_u + n_l\phi_l}\right)^3 + \frac{n_l}{a_l^2}\left(\frac{\phi_l}{n_u\phi_u + n_l\phi_l}\right)^3\right\}. \tag{2.11}$$

For the readability we recall the definition of ϕ_t and ϕ_c given in (2.5) here

$$\phi_u := \frac{\pi(R_{1u} - R_{0u})t_u^3}{6\mu L_m \log\left(\frac{2(R_{1u}-R_{0u})}{2R_{0u}-t_u} + 1\right)}, \qquad \phi_l := \frac{\pi(R_{1l} - R_{0l})t_l^3}{6\mu L_m \log\left(\frac{2(R_{1l}-R_{0l})}{2R_{0l}-t_l} + 1\right)},$$

where t_u and t_l are given by

$$t_l := t_{l0} + \frac{R_{l1} - R_{l0}}{L_m}(u_l - u_m), \quad t_u := t_{u0} + \frac{R_{u1} - R_{u0}}{L_m}(u_u - u_m). \tag{2.12}$$

Since a_u and a_l are the channel areas at the exit of flow path of the main piston, we need to separate the cases according to the positivity or negativity of $\partial_t u_m$. Indeed, recalling Figures 3 and 4, a_u and a_l are the areas of lower sides when $\partial_t u_m \geq 0$ and are the areas of upper sides when $\partial_t u_m \leq 0$. Note that the area of a donut-shaped region with outer diameter R and inner diameter $R - t$ is given by $\pi R^2 - \pi(R-t)^2 = \pi t(2R - t)$, then we see that

$$a_u = \begin{cases} \pi t_u(2R_{0u} - t_u), & \text{if } \partial_t u_m \geq 0, \\ \pi t_u(2R_{1u} - t_u), & \text{if } \partial_t u_m \leq 0, \end{cases} \quad a_l = \begin{cases} \pi t_l(2R_{0l} - t_l), & \text{if } \partial_t u_m \geq 0, \\ \pi t_l(2R_{1l} - t_l), & \text{if } \partial_t u_m \leq 0. \end{cases}$$

Consequently, we obtain the mathematical model of the damper. Namely, the output F_d is given from the input function u_m by solving the nonlinear

ordinary differential equations (2.7)–(2.8). Remark that it is not trivial that the solutions u_u and u_l for the Equations (2.7) and (2.8) are obtained explicitly, because the nonlinear terms are not standard polynomials due to including the absolute values. Even if we can find the explicit solution formula, the formula for calculating the value of F_d is complicated, so it is more realistic to calculate it numerically than theoretically. In what follows, we introduce a scheme for obtaining numerical solutions of the nonlinear ordinary differential equations (2.7)–(2.8) and error estimate for the approximate solutions.

3 Numerical methods

Each of the Equations (2.7) and (2.8) is written as

$$M_i\partial_t^2 u_i + C_i\partial_t u_i + \tilde{C}_i|\partial_t u_i|\partial_t u_i + K_i u_i = K_i u_m,$$

for $i = u, l$. Obviously, the each equation of (2.7) and (2.8) is solved independently for given u_m. Then let us consider the equation:

$$M\partial_t^2 u + C\partial_t u + \tilde{C}|\partial_t u|\partial_t u + Ku = f, \tag{3.1}$$

for given function f. Setting $v := \partial_t u$, the Equation (3.1) can be decomposed to the system of first order differential equations:

$$\begin{cases} \partial_t u = v, \\ M\partial_t v = -Cv - \tilde{C}|v|v - Ku + f. \end{cases} \tag{3.2}$$

We give the mathematical analysis for the system such as error estimate between strict solution $(u, v)^t$ and an approximate solution by using the structure-preserving numerical method given below. Regarding the system (3.2) as $\partial_t \boldsymbol{u} = \boldsymbol{g}(\boldsymbol{u})$ for $\boldsymbol{u} := (u, v)^t$, $\boldsymbol{g}(\boldsymbol{u}) := (v, (-Cv - h(v) - Ku + f)/M)^t$ with $h(v) := \tilde{C}|v|v$, such the Runge-Kutta method seems to be more applicable and efficient. However, we should remark that $\boldsymbol{g}$ is not sufficient smooth. Indeed, to utilize the error estimate of the order $O(\Delta t^4)$, it requires C^4-regularity for u. On the other hand, it is easily seen that $h \neq C^4$ but $h \in C^{1,1}$. Then the C^4-regularity for the solution is not assured. This is the reason why we shall use the structure-preserving numerical method. Multiplying v by the second equation derives the following energy law:

$$\partial_t \left(\frac{M}{2} v^2 + \frac{K}{2} u^2 \right) + Cv^2 + \tilde{C}|v|^3 = vf. \tag{3.3}$$

Integrating over $t \in [0, t]$, we obtain the total energy conservation law:

$$\begin{aligned} \frac{M}{2} v^2(t) + \frac{K}{2} u^2(t) + \int_0^t \left(Cv^2(s) + \tilde{C}|v|^3(s) \right) ds \\ = \int_0^t v(s) f(s) ds + \frac{M}{2} v^2(0) + \frac{K}{2} u^2(0). \end{aligned}$$

The Young inequality $ab \le \tilde{C}a^3 + \frac{2}{3\sqrt{3\tilde{C}}}b^{3/2}$ implies the a priori estimate (energy estimate) for the solutions as follows:

$$\max_{t\in[0,T]}\left(\frac{M}{2}v^2(t)+\frac{K}{2}u^2(t)\right)+C\int_0^T v^2(t)dt \le \frac{M}{2}v^2(0)+\frac{K}{2}u^2(0)+\frac{2}{3\sqrt{3\tilde{C}}}\int_0^T |f|^{\frac{3}{2}}(t)dt.$$

Let $(U_n, V_n)^t$ be the solution for the numerical scheme corresponding to the solution $(u, v)^t$ at $t = n\Delta t$ with the time splitting size Δt. Our numerical scheme is as follows:

$$\begin{cases} \frac{U_{n+1}-U_n}{\Delta t} = \frac{V_{n+1}+V_n}{2}, \\ M\frac{V_{n+1}-V_n}{\Delta t} = -C\frac{V_{n+1}+V_n}{2} - \tilde{C}\left|\frac{V_{n+1}+V_n}{2}\right|\frac{V_{n+1}+V_n}{2} \\ \qquad\qquad -K\frac{U_{n+1}+U_n}{2} + f_{n+\frac{1}{2}}, \end{cases} \tag{3.4}$$

where $f_{n+\frac{1}{2}} := f\left(\left(n+\frac{1}{2}\right)\Delta t\right)$. The scheme inherits the above energy conservation law in the following sense. Multiplying $\frac{V_{n+1}+V_n}{2}$ by the second equation yields

$$\frac{1}{\Delta t}\left\{\left(\frac{M}{2}|V_{n+1}|^2+\frac{K}{2}|U_{n+1}|^2\right)-\left(\frac{M}{2}|V_n|^2+\frac{K}{2}|U_n|^2\right)\right\} + C\left(\frac{V_{n+1}+V_n}{2}\right)^2+\tilde{C}\left|\frac{V_{n+1}+V_n}{2}\right|^3 = \frac{V_{n+1}+V_n}{2}\cdot f_{n+\frac{1}{2}},$$

which corresponds to (3.3). In a similar fashion as above, summing the equation from $n = 0$ to $n = n-1$, we obtain the discrete version of the energy conservation law:

$$\frac{M}{2}|V_n|^2+\frac{K}{2}|U_n|^2+\sum_{\ell=0}^{n-1}\left\{C\left(\frac{V_{\ell+1}+V_\ell}{2}\right)^2+\tilde{C}\left|\frac{V_{\ell+1}+V_\ell}{2}\right|^3\right\}\Delta t = \sum_{\ell=0}^{n-1}\frac{V_{\ell+1}+V_\ell}{2}\cdot f_{\ell+\frac{1}{2}}\Delta t+\frac{M}{2}|V_0|^2+\frac{K}{2}|U_0|^2, \tag{3.5}$$

and using the Young inequality

$$\max_{n=0,1,\dots,N}\left(\frac{M}{2}|V_n|^2+\frac{K}{2}|U_n|^2\right)+C\sum_{n=0}^{N-1}\left(\frac{V_{n+1}+V_n}{2}\right)^2\Delta t \le \frac{2}{3\sqrt{3\tilde{C}}}\sum_{n=0}^{N-1}\left|f_{n+\frac{1}{2}}\right|^{\frac{3}{2}}\Delta t+\frac{M}{2}|V_0|^2+\frac{K}{2}|U_0|^2.$$

In this sense, the finite difference scheme (3.4) is called the *structure-preserving numerical scheme*. We remark that the scheme possesses the property of the *symplectic integrator*, and is also identified with the so-called *mid-point rule*.

3.1 Existence of solution

Let us discuss the existence and uniqueness of solution for (3.4). In general, it is not trivial that the system of nonlinear equations has a unique solution. However, in the case of our equation, it is almost trivial because the system is almost quadratic. Nevertheless, we introduce the existence of a solution because it will be used as the actual numerical simulations.

Set $V := \frac{V_{n+1}+V_n}{2}$ and $U := \frac{U_{n+1}+U_n}{2}$. Then the system (3.4) is rewritten as

$$\begin{aligned} \frac{2}{\Delta t}U - \frac{2}{\Delta t}U_n =& V, \\ \frac{2M}{\Delta t}V - \frac{2M}{\Delta t}V_n =& -CV - \tilde{C}|V|V - KU + f_{n+\frac{1}{2}}. \end{aligned} \tag{3.6}$$

Eliminating U from the system, we obtain the equation for V;

$$\tilde{C}|V|V + \left(\frac{2M}{\Delta t} + \frac{K\Delta t}{2} + C\right)V + \left(KU_n - \frac{2M}{\Delta t}V_n - f_{n+\frac{1}{2}}\right) = 0.$$

Let us furthermore denote $\left(\frac{2M}{\Delta t} + \frac{K\Delta t}{2} + C\right)/\tilde{C}$ and $\left(KU_n - \frac{2M}{\Delta t}V_n - f_{n+\frac{1}{2}}\right)/\tilde{C}$ by α and β, respectively. Thus, the resulting equation is $|V|V + \alpha V + \beta = 0$. Since

$$y = \begin{cases} V^2 + \alpha V + \beta, & V \geq 0, \\ -V^2 + \alpha V + \beta, & V < 0, \end{cases}$$

we thus obtain

$$\frac{dy}{dV} = \begin{cases} 2V + \alpha, & V \geq 0, \\ -2V + \alpha, & V < 0. \end{cases}$$

Observe that $\alpha \geq (2\sqrt{MK}+C)/\tilde{C} > 0$ from the arithmetic mean and geometric mean inequality. Then it holds that $\frac{dy}{dV} \geq \alpha > 0$ for any $V \in \mathbb{R}$. Therefore, we conclude that the Equation (3.6) has a unique solution V. Namely, for given $(U_n, V_n)^t$ and f, there exists a unique solution $(U_{n+1}, V_{n+1})^t$ for the Equations (3.4). The existence of a solution $(U_n, V_n)^t$ for given $(U_0, V_0)^t$ follows from the inductive argument. More concretely, we have the explicit formula:

$$V = \begin{cases} \frac{-\alpha+\sqrt{\alpha^2-4\beta}}{2}, & \beta < 0, \\ \frac{\alpha-\sqrt{\alpha^2+4\beta}}{2}, & \beta \geq 0. \end{cases}$$

Consequently, in the actual numerical simulation, our scheme is calculated as follows:

Theorem 1 [Algorithm]. *The solution for* (3.4) *is calculated by the following scheme. For each n, we first calculate $\alpha = \left(\frac{2M}{\Delta t} + \frac{K\Delta t}{2} + C\right)/\tilde{C}$ and $\beta = \left(KU_n - \frac{2M}{\Delta t}V_n - f_{n+\frac{1}{2}}\right)/\tilde{C}$. Next, we calculate V_{n+1} and U_{n+1} as follows.*

(i) In the case $\beta < 0$,

$$V_{n+1} = -\alpha + \sqrt{\alpha^2 - 4\beta} - V_n, \qquad U_{n+1} = U_n + \frac{V_{n+1} + V_n}{2}\Delta t;$$

(ii) In the case $\beta \geq 0$,

$$V_{n+1} = \alpha - \sqrt{\alpha^2 + 4\beta} - V_n, \qquad U_{n+1} = U_n + \frac{V_{n+1} + V_n}{2}\Delta t.$$

3.2 Error estimate

We denote the error $(U_n - u(n\Delta t), V_n - v(n\Delta t))$ by $(e_{1,n}, e_{2,n})$. We obtain the following error estimate which does not require the smallness assumption for Δt in spite of the fact that the problem is nonlinear. The error estimate corresponds to the estimate given in [17] as the *unconditional error estimate*.

Theorem 2. *Let N be arbitrarily fixed and $T := N\Delta t$. Then for any $\Delta t > 0$, there exists a constant such that*

$$\max_{n=0,1,\ldots,N} (|e_{1,n}| + |e_{2,n}|) \leq c\sqrt{T}|\Delta t|^2.$$

Proof. Subtracting (3.4) from (3.2) at $t = (n + 1/2)\Delta t$, we can derive the equations for errors:

$$\frac{e_{1,n+1} - e_{1,n}}{\Delta t} = \frac{e_{2,n+1} + e_{2,n}}{2} + \zeta_{1,n}, \tag{3.7}$$

$$\begin{aligned} M\left(\frac{e_{2,n+1} - e_{2,n}}{\Delta t}\right) =& - C\left(\frac{e_{2,n+1} + e_{2,n}}{2}\right) - K\left(\frac{e_{1,n+1} + e_{1,n}}{2}\right) \\ & - \left\{h\left(\frac{V_{n+1} + V_n}{2}\right) - h\left(\frac{V_{n+1} + V_n}{2}\right)\right\} + \zeta_{2,n}, \end{aligned} \tag{3.8}$$

where for $u_n = u(n\Delta t)$, $v_n = v(n\Delta t)$ and

$$\begin{aligned} \zeta_{1,n} :=& \left\{(\partial_t u)\left(\left(n + \frac{1}{2}\right)\Delta t\right) - \frac{u_{n+1} - u_n}{\Delta t}\right\} + \left(\frac{u_{n+1} + u_n}{2} - u_{n+\frac{1}{2}}\right), \\ \zeta_{2,n} :=& M\left\{(\partial_t v)\left(\left(n + \frac{1}{2}\right)\Delta t\right) - \frac{v_{n+1} - v_n}{\Delta t}\right\} + C\left(\frac{v_{n+1} + v_n}{2} - v_{n+\frac{1}{2}}\right) \\ & - K\left(\frac{u_{n+1} + u_n}{2} - u_{n+\frac{1}{2}}\right) - \left\{h\left(\frac{v_{n+1} + v_n}{2}\right) - h\left(v_{n+\frac{1}{2}}\right)\right\}. \end{aligned}$$

Since $h(v) := \tilde{C}|v|v \in C^{1,1}$, the boundedness of $\partial_t^2 u$, $\partial_t^3 u$ and $\partial_t^2 v$, $\partial_t^3 v$ are assured. Indeed, from the energy estimate and the equation the boundedness of $\partial_t u$ and $\partial_t v$ is trivial. Furthermore, from the equation, we see that $\partial_t^2 v = -\partial v + h'(v)\partial_t v - \partial_t u - f'$. Then the boundedness of $\partial_t^2 v$ are derived and the one for $\partial_t^2 u$ is also obvious from the first equation of (3.2). Remark that $h'(v) = 2\tilde{C}|v|$ is the Lipschitz continuous, then there exists some constant L such that $|h'(v_1) - h'(v_2)| \leq L|v_1 - v_2|$ with for any v_1 and v_2. Since

$$\begin{aligned} & \sup_{t\in[0,T]} \left|\lim_{\tau\to 0} \frac{h'(v(t+\tau))(\partial_t v)(t+\tau) - h'(v(t))\partial_t v(t)}{\tau}\right| \\ & \quad \leq \sup_{t\in[0,T]} \left|h'(v(t))\partial_t^2 v(t)\right| + \sup_{t\in[0,T]} \partial_t v(t) \cdot \left|\lim_{\tau\to 0} \frac{h'(v(t+\tau)) - h'(v(t))}{\tau}\right| \\ & \quad \leq \sup_{t\in[0,T]} |h'(v(t))| \cdot \sup_{t\in[0,T]} \left|\partial_t^2 v(t)\right| + L \sup_{t\in[0,T]} |\partial_t v(t)|^2, \end{aligned}$$

we obtain the boundedness of $\partial_t^3 v$ and hence also of $\partial_t^3 u$. From the Taylor theorem, there exist constants c such that

$$\begin{aligned}\frac{u_{n+1}+u_n}{2} - u_{n+\frac{1}{2}} =& \Delta t^2 \cdot \partial_t^2 u(c),\\ \partial_t u\left(\left(n+\frac{1}{2}\right)\Delta t\right) - \frac{u_{n+1}-u_n}{\Delta t} =& -\Delta t^2 \cdot \partial_t^3 u(c),\\ h\left(\frac{v_{n+1}+v_n}{2}\right) - h\left(v_{n+\frac{1}{2}}\right) =& h'(c)\cdot\left(\frac{v_{n+1}+v_n}{2} - v_{n+\frac{1}{2}}\right),\end{aligned}$$

where the constants c differ each other line by line. Therefore, we obtain

$$\zeta_{1,n} = O(\Delta t^2), \quad \zeta_{2,n} = O(\Delta t^2).$$

Multiplying $\frac{e_{2,n+1}+e_{2,n}}{2}$ by (3.8) and using (3.7) yield

$$\begin{aligned}&\frac{1}{\Delta t}\left\{\left(\frac{K}{2}|e_{1,n+1}|^2 + \frac{M}{2}|e_{2,n+1}|^2\right) - \left(\frac{K}{2}|e_{1,n}|^2 + \frac{M}{2}|e_{2,n}|^2\right)\right\}\\ &+ C\left|\frac{e_{2,n+1}+e_{2,n}}{2}\right|^2 + \left\{h\left(\frac{V_{n+1}+V_n}{2}\right) - h\left(\frac{v_{n+1}+v_n}{2}\right)\right\}\cdot\frac{e_{2,n+1}+e_{2,n}}{2}\\ &= \frac{e_{1,n+1}+e_{1,n}}{2}\cdot\zeta_{1,n} + \frac{e_{2,n+1}+e_{2,n}}{2}\cdot\zeta_{2,n}.\end{aligned}$$

Since $h'(u) \geq 2\tilde{C}|u| \geq 0$, we have from the mean value theorem that

$$\begin{aligned}&\left\{h\left(\frac{V_{n+1}+V_n}{2}\right) - h\left(\frac{v_{n+1}+v_n}{2}\right)\right\}\cdot\frac{e_{2,n+1}+e_{2,n}}{2}\\ &\geq h'(c)\cdot\left|\frac{e_{2,n+1}+e_{2,n}}{2}\right|^2 \geq 0.\end{aligned}$$

We thus obtain that

$$\begin{aligned}&\frac{1}{\Delta t}\left\{\left(\frac{K}{2}|e_{1,n+1}|^2 + \frac{M}{2}|e_{2,n+1}|^2\right) - \left(\frac{K}{2}|e_{1,n}|^2 + \frac{M}{2}|e_{2,n}|^2\right)\right\}\\ &\qquad + C\left|\frac{e_{2,n+1}+e_{2,n}}{2}\right|^2\\ &\leq \left|\frac{e_{2,n+1}+e_{2,n}}{2}\right|\cdot|\zeta_{2,n}| + \left|\frac{e_{1,n+1}+e_{1,n}}{2}\right|\cdot|\zeta_{1,n}|\\ &\leq \left|\frac{e_{2,n+1}+e_{2,n}}{2}\right|\cdot|\zeta_{2,n}| + \left|\frac{e_{2,n+1}+e_{2,n}}{2}\right|\cdot|\zeta_{1,n}| + |\zeta_{2,n}|\cdot|\zeta_{1,n}|\\ &\leq C\left|\frac{e_{2,n+1}+e_{2,n}}{2}\right|^2 + \frac{1}{2C}\left(|\zeta_{1,n}|^2 + |\zeta_{1,n}|^2\right) + |\zeta_{2,n}|\cdot|\zeta_{1,n}|,\end{aligned}$$

then

$$\frac{1}{\Delta t}\left\{\left(\frac{K}{2}|e_{1,n+1}|^2 + \frac{M}{2}|e_{2,n+1}|^2\right) - \left(\frac{K}{2}|e_{1,n}|^2 + \frac{M}{2}|e_{2,n}|^2\right)\right\} \leq c|\Delta t|^4.$$

Summing up these inequality from $n = 0$ to $n = n - 1$ yields

$$\max_{n=0,1,\ldots,N} \left(\frac{K}{2}|e_{1,n}|^2 + \frac{M}{2}|e_{2,n}|^2 \right) \leq cT|\Delta t|^4,$$

which completes the proof. □

4 Numerical simulation

In this section, we confirm the behavior of solution through several numerical simulations of F_d for given u_m, which is calculated by (2.9), where the functions u_r and u_l are calculated by solving (2.7) and (2.8). We give the input function u_m and the initial values of $u_u = u_{u0}$, $\partial_t u_u = u_{u1}$, $u_l = u_{l0}$ and $\partial_t u_l = u_{l1}$. By the scheme (3.4), namely, by the manner given in Theorem 1, we calculate $(U_{u,n}, V_{u,n})$ and $(U_{l,n}, V_{l,n})$ which are approximate values of $(u_u, \partial_t u_u)$ and $(u_l, \partial_t u_l)$. From the values $V_{u,n}$ and $V_{l,n}$, we calculate $F_{d,n}$ by (2.9)–(2.12) with (2.5), which corresponds to the value of F_d.

In actual numerical calculations, the constraints $t_u \geq 0$ and $t_l \geq 0$ are imposed. Moreover, $R_{l1} < R_{l0}$ and $R_{u1} > R_{u0}$ should be satisfied by the geometrical structure. Then these conditions are rewritten as

$$u_u \geq u_m - \frac{L_m t_{u0}}{R_{u1} - R_{u0}}, \qquad u_l \leq u_m - \frac{L_m t_{l0}}{R_{l1} - R_{l0}}. \tag{4.1}$$

To fulfill these conditions, if the numerical solution $U_{u,n+1}$ calculated by the scheme given in Theorem 1 offends from the condition, namely, indicates $U_{u,n+1} < u_{m,n+1} - \frac{L_m t_{u0}}{R_{u1} - R_{u0}}$, we compensate by substituting $u_{m,n+1} - \frac{L_m t_{u0}}{R_{u1} - R_{u0}}$ for $U_{u,n+1}$. Similarly, if $U_{l,n+1}$ satisfies $U_{l,n+1} > u_{m,n+1} - \frac{L_m t_{l0}}{R_{l1} - R_{l0}}$, then we substitute $u_{m,n+1} - \frac{L_m t_{l0}}{R_{l1} - R_{l0}}$ for $U_{l,n+1}$. We note that the error estimate for the approximate solution with this compensation is not given in Section 3. Indeed, if the constraint is violated in numerical simulations, then the energy structure is broken. However, it is too complicated to consider the structure-preserving numerical scheme with the constraint. Then here we restrict ourselves to considering the error estimate for the numerical solution without the constraints.

The parameters used in the numerical calculations are listed in Table 1. These are based on the parameters used on the actual damper.

Table 1. Parameters for the numerical simulations.

$\rho = 0.835$ [kg/m^3]	$R_{l1} = 0.004/2$ [m]	$C_d = 0.7$, $n_s = 16$
$\mu = 0.0266$ [Pa · s]	$R_{u0} = 0.0031/2$ [m]	$r_u = r_l = 0.0002/2$ [m]
$L = 0.01$[m]	$R_{u1} = 0.0046/2$ [m]	$L_u = L_l = 0.001$ [m]
$A = (0.0465)^2\pi/4$[m^2]	$R_{l0} = 0.0055/2$ [m]	$K_u = K_l = 25240$ [N/m]
$n_u = n_l = 2$	$t_{u0} = t_{l0} = 0.00018$ [m]	$M_u = M_l = 0.04$ [kg]

Let us demonstrate several examples of numerical simulations. Throughout the calculation, we set the time stepping size Δt as 0.0001.

- **Case 1 (linearly increasing input velocity).**
We first study the case that the input is

$$u_m(t) = 0.02t^2, \quad \partial_t u_m(t) = 0.04t,$$

which means the velocity of the input $\partial_t u_m$ increases linearly. We set all the initial values of the sub-pistons u_{u0}, u_{u1}, u_{l0}, u_{l1} are zeros, and $T = 10$.

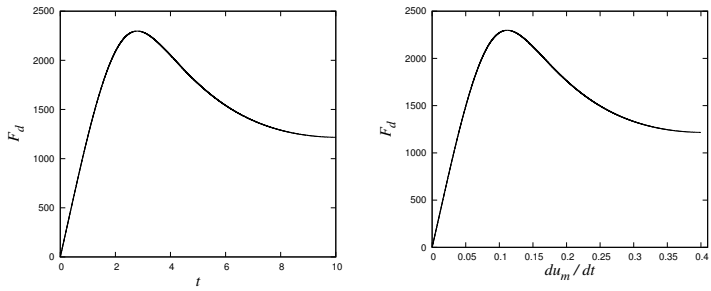

(a) the relation of $t - F_d$ (b) the relation of $\partial_t u_m - F_d$

Figure 8. The solution in Case 1.

The relation between time t and output F_d and the relation between input $\partial_t u_m$ and F_d are shown in Figure 8. Although the shape of both graphs is similar due to the monotonically increasing input, it can be observed that the output decreases at higher speeds, indicating that the targeted decrease in damping force at higher speeds is realized. The energy change of the sub-pistons P_u and P_l is shown in Figure 11 (a). Because of the monotonous increase to the upper direction, the upper piston offends the constraint (4.1) in the middle, and the relation of energy conservation is broken. On the other hand, the lower piston is not particularly affected by the condition, so the energy conservation relation (3.5) is satisfied.

- **Case 2 (oscillating input velocity).**
Next, we examine the following input oscillating at the frequency of $f = 0.2$,

$$u_m(t) = \frac{1}{2}\left(1 - \cos\left(2\pi f t\right)\right), \qquad \partial_t u_m(t) = \pi f \sin\left(2\pi f t\right).$$

Here, we also calculate it under the assumptions u_{u0}, u_{u1}, u_{l0}, u_{l1} are zero, but $T = 6$. The behavior of the solution and the energy change are shown in Figure 9 and Figure 11 (b).

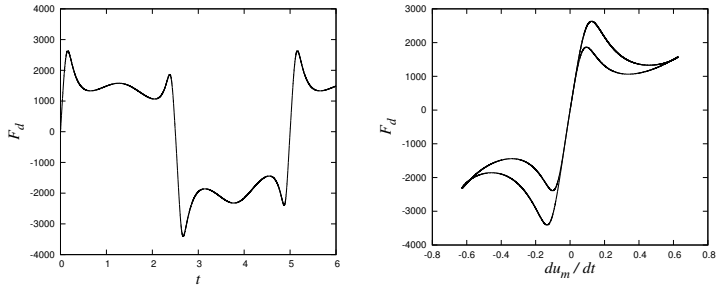

(a) the relation of $t - F_d$ (b) the relation of $\partial_t u_m - F_d$

Figure 9. The solution in Case 2.

When the input oscillates, the brake is applied when the velocity exceeds a certain speed, but the brake is also applied midway because it turns to decrease midway due to the effect of dynamic resistance, but the brake is significantly decreased again due to the effect of dynamic pressure resistance. The relation between the input velocity $\partial_t u_m$ and F_d draws a hysteresis loop. The energy conservation laws are broken due to offending the conditions (4.1).

- **Case 3 (small oscillating input velocity).**
  As the last example, we consider the case where the input oscillates ($f = 0.2$) but its amplitude is small such as

$$u_m(t) = \frac{1}{10}\left(1 - \cos\left(2\pi f t\right)\right), \qquad \partial_t u_m(t) = \frac{\pi f}{5}\sin\left(2\pi f t\right).$$

The relation between t and F_d and the relation between $\partial_t u_m$ and F_d are shown in Figure 10. In this case, the solutions do not offend the constraint (4.1), then we observe that the energy conservation law (3.5) holds. We also st $T = 6$, but for the visibility of energy change, we set the initial values as follows: $u_{u0} = 0.0001$, $u_{u1} = 0$, $u_{l0} = -0.00011$ and $u_{l1} = 0$. As shown in Figure 11 (c), we can confirm that the energy conservation law (3.5) holds when the amplitude is sufficiently small.

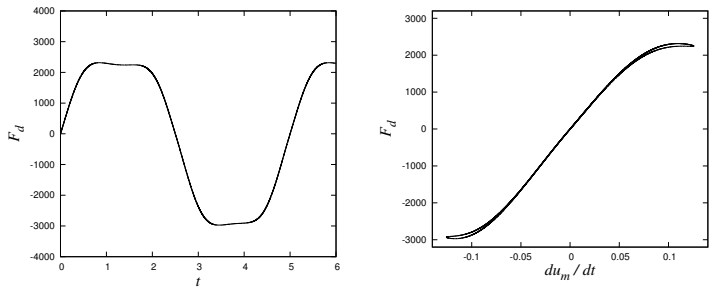

(a) the relation of $t - F_d$ (b) the relation of $\partial_t u_m - F_d$

Figure 10. The solution in Case 3.

The following graphs indicate the relation between time and energies for the sub-pistons.

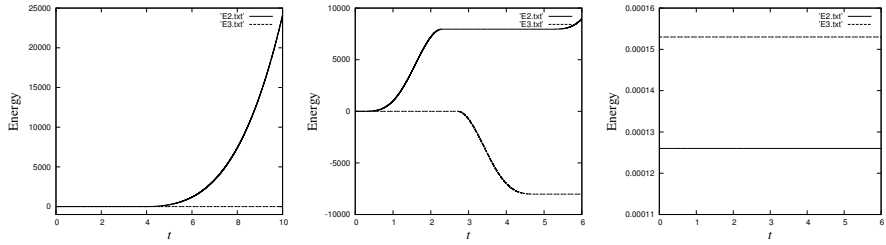

(a) Case 1 (b) Case 2 (c) Case 3

Figure 11. The energy of the sub-pistons.

5 Concluding remarks

We study the mechanical passive damper of which resistance force decreases by the increasing of velocity. In this article, we derive the mathematical model of the damper taking the dynamic pressure (hydrodynamic) resistance into account. One of the problems is the complexity of the fluid paths of the main-piston. To enable us to get a mathematical model, we propose the assumption given in (2.6). Although this is an empirical rule and not a theoretically derived law, we argued for its validity by comparing it with CFD. By adapting the hypothesis, the mathematical model is derived. On the other hand, since the dynamic pressure resistance is generally nonlinear effect, the derived models are nonlinear ordinary differential equations. It is not trivial to solve the equations explicitly. We thus give the numerical scheme to solve the nonlinear ordinary differential equations in Theorem 1, and we also give an error estimate which assures the validity of the numerical solution. Lastly, we also demonstrate several numerical simulations and confirm that the solution behaves as intended. The analysis for the structure-preserving numerical scheme with the constraint (4.1) still remains open.

Acknowledgements

This work was partially supported by JSPS KAKENHI Grant Numbers JP20K03687 and JP20KK0308. The authors would like to thank the anonymous reviewers for their kind and instructive comments.

References

[1] V.I. Arnold. *Ordinary Differential Equations*. Springer-Verlag, Berlin, 2006.

[2] V. Barbu. *Differential Equations*. Springer, Cham, 2016. https://doi.org/10.1007/978-3-319-45261-6.

[3] J. D. Carlson. Innovative devices that enable semi-active control. *Proceeding of the 3rd World Conference on Structural Control*, pp. 227–236, 2003.

[4] J. Dixon. *The Shock Absorber Handbook*. Wiley-professional Engineering Publishing Series, 2007. https://doi.org/10.1002/9780470516430.

[5] S. Duym and K. Reybrouck. Physical characterization of nonlinear shock absorber dynamics. *Proceeding of the 3rd World Conference on Structural Control*, **43**(4):181–188, 1998.

[6] D. Furihata and T. Matsuo. *Discrete Variational Derivative Method*. CRC Press/Taylor Francis, 2010. https://doi.org/10.1201/b10387.

[7] E. Hairer, C. Lubich and G. Wanner. *Geometric Numerical Integration. Structure-Preserving Algorithms for Ordinary Differential Equations*. Springer-Verlag, Berlin, 2006.

[8] M. Hayashi, H. Kato, T. Kusumoto and T. Sukegawa. Development of double piston shock absorber. *Journal of Society of Automotive Engineers of Japan*, **64**(7):63–66, 2010.

[9] F. Herr, T. Mallin, J. Lane and S. Roth. A shock absorber model using CFD analysis and easy. *SAE Steering and Suspension Technology Symposium*, **5**:267–281, 1999. https://doi.org/10.4271/1999-01-1322.

[10] K Hio, Y. Suda, T. Shiba, T. Kondo and H. Yamagata. A study on nonlinear damping force characteristics of electromagnetic damper for automobiles. *Journal of Society of Automotive Engineers of Japan*, **35**(1):162–172, 2004.

[11] T. Murakami, M. Sakai and M. Nakano. Development of a passive type MR damper with variable damping characteristics dependent on the displacement and velocity. *Transactions of the Japan Society of Mechanical Engineers, Series C*, **77**(774):257–269, 2011. https://doi.org/10.1299/kikaic.77.257.

[12] K. Reybrouck. A nonlinear parametric model of a automotive shock absorber. *SAE Paper*, p. No. 9400869, 1994. https://doi.org/10.4271/940869.

[13] M. Shams, R. Ebrahimi, A. Raoufi and B. J. Jafari. CFD-FEA analysis of hydraulic shock absorber valve behavior. *Int. J. Auto. Tech.*, **8**(5):615–622, 2007.

[14] C. Surace, K. Worden and G. R. Tomlinson. An improved nonlinear model for an automotive shock absorber. *Nonlinear Dynamics*, **3**(6):413–429, 1992. https://doi.org/10.1007/BF00045646.

[15] D. Watanabe and H. Okamura. Development of a mechanical passive damper whose damping force decreases with increasing piston speed and study on its modelling. *Transactions in the JAME (in Japanese)*, **84**:18–00138, 2018. https://doi.org/10.1299/transjsme.18-00138.

[16] S. Yoshikawa. Energy method for structure-preserving finite difference schemes and some properties of difference quotient. *J. Comput. Appl. Math.*, **311**:394–413, 2017. https://doi.org/10.1016/j.cam.2016.08.008.

[17] S. Yoshikawa. Remarks on energy methods for structure-preserving finite difference schemes-small data global existence and unconditional error estimate. *Appl. Math. Comput.*, **341**:80–92, 2019. https://doi.org/10.1016/j.amc.2018.08.030.